Int. J. Radiation Oncology Biol. Phys., Vol. 63, No. 4, pp. 1245–1251, 2005

0360-3016/05/$–see front matter

doi:10.1016/j.ijrobp.2005.07.971

BIOLOGY CONTRIBUTION

CHANGES IN THE TUMOR MICROENVIRONMENT DURING LOW-DOSE-RATE PERMANENT SEED IMPLANTATION IODINE-125 BRACHYTHERAPY

Greg O. Cron, Ph.D.,* Nelson Beghein, B.Sc.,*† Nathalie Crokart, M.Sc.,*† Emilie Chavée, B.Sc.,*† Sabine Bernard, M.Sc.,‡ Stefaan Vynckier, Ph.D.,‡ Pierre Scalliet, M.D., Ph.D.,‡ and Bernard Gallez, Ph.D.*†

*Laboratory of Biomedical Magnetic Resonance, †Laboratory of Medicinal Chemistry and Radiopharmacy, and ‡Department of Radiation Oncology, Université Catholique de Louvain, Brussels, Belgium

Purpose: There is a lack of data regarding how the tumor microenvironment (e.g., perfusion and oxygen partial pressure [pO_2]) changes in response to low-dose-rate (LDR) brachytherapy. This may be why some clinical issues remain unresolved, such as the appropriate use of adjuvant external beam radiation therapy (EBRT). The purpose of this work was to obtain some basic preclinical data on how the tumor microenvironment evolves in response to LDR brachytherapy.

Methods and Materials: In an experimental mouse tumor, pO_2 (measured by electron paramagnetic resonance) and perfusion (measured by dynamic contrast-enhanced magnetic resonance imaging) were monitored as a function of time (0–6 days) and distance (0–2 mm and 2–4 mm) from an implanted 0.5 mCi iodine-125 brachytherapy seed.

Results: For most of the experiments, including controls, tumors remained hypoxic at all times. At distances of 2–4 mm from radioactive seeds (~1.5 Gy/day), however, there was an early, significant increase in pO_2 within 24 h. The pO_2 in that region remained elevated through Day 3. Additionally, the perfusion in that region was significantly higher than for controls starting at Day 3.

Conclusions: It may be advantageous to give adjuvant EBRT shortly (~1 to 2 days) after commencement of clinical LDR brachytherapy, when the pO_2 in the spatial regions between seeds should be elevated. If chemotherapy is given adjuvantly, it may best be administered just a little later (~3 or 4 days) after the start of LDR brachytherapy, when perfusion should be elevated.

INTRODUCTION

Low-dose-rate (LDR) brachytherapy via permanently implanted iodine-125 or palladium-103 seeds (~30 keV photons having a dose reduction factor of 10 for <1 cm of tissue) is frequently used to treat tumors, especially prostate cancer. Advances in image-guided placement of the seeds have enabled physicians to use this technique to deliver conformal radiation doses to tumor tissue, resulting in good success rates for local control and significant sparing of normal tissues (1–4).

Despite the relative success of LDR brachytherapy, issues remain regarding the optimal dose, isotope, use of planning treatment margins, and use of adjuvant therapies such as external beam radiation therapy (EBRT) (5–8). These uncertainties may stem, at least in part, from the lack of data regarding how the tumor microenvironment (e.g., perfusion and oxygen partial pressure [pO_2]) changes in response to LDR brachytherapy. For example, the variation of pO_2 in the tumor as a function of time may be an important consideration for the timing of adjuvant EBRT, because oxygen is a powerful radiosensitizer (9, 10).

There have been some studies which have correlated pretreatment tumor perfusion or pO_2 with treatment outcome (11–14). However, few of these studies have dealt with LDR brachytherapy and none of them have followed changes in tumor pO_2 as a function of time. van den Berg *et al.* studied changes in perfusion and pO_2 in an experimental rat tumor as a function of time during the first 24 h after implantation of high-energy, high-dose-rate (300 keV, 300 Gy per hour) iridium-192 brachytherapy sources (10). Additionally, there have been a few studies which have measured changes in pO_2 and perfusion as a function of time after a single, large (> ~10 Gy), dose of EBRT (15–24). However, none of these data may be readily applicable to LDR brachytherapy, where the dose is highly localized

Reprint requests to: Bernard Gallez, Ph.D., CMFA/REMA, Avenue Mounier 73.40, B-1200 Brussels, Belgium. Tel: (+32) 2-7642792; Fax: (+32) 2-7642790; E-mail: Gallez@cmfa.ucl.ac.be

This work is supported by grants from the Belgian National Fund for Scientific Research (FNRS), the Télévie, the Fonds Joseph Maisin, and the "Actions de Recherches Concertées-Communauté Française de Belgique-ARC 04/09–317." E.C. and S.B. are FNRS-Télévie Fellows.

Acknowledgment—The authors thank Guerbet Laboratories (Roissy, France) for providing P792.

Received Mar 23, 2005, and in revised form July 15, 2005. Accepted for publication July 24, 2005.

inside the tumor (often with significant dose gradients) and the dose rates during delivery of the radiation are approximately 3 orders of magnitude smaller than for EBRT (i.e., several Gy per day vs. several Gy in minutes).

Powerful tools have become recently available for studying the tumor microenvironment *in vivo*. Contrast-enhanced magnetic resonance imaging (MRI) may be used to measure tumor perfusion noninvasively (25, 26). Moreover, recent advances in electron paramagnetic resonance (EPR) have made it possible to monitor pO_2 *in vivo* repeatedly and relatively noninvasively (27).

The purpose of this work was to obtain some basic preclinical data on how the tumor microenvironment evolves in response to LDR brachytherapy. In an experimental mouse tumor, pO_2 (using EPR) and perfusion (using MRI) were measured as a function of time and distance from an implanted LDR iodine-125 brachytherapy seed.

METHODS AND MATERIALS

Transplantable liver tumors (TLT) were implanted in the gastrocnemius muscle in the leg of male NMRI mice (20–25 g, B&K, Hull, UK) (28). Brachytherapy seeds were implanted when the tumors reached a diameter of 8.0 ± 0.5 mm. All experiments were performed according to national animal care regulations.

Mice were anesthetized by inhalation of isoflurane mixed with air in a continuous flow (1.8 L/h), delivered by a nose cone. Anesthesia was initiated using 3% isoflurane and stabilized at 1.6% isoflurane for at least 10 min before any manipulation.

Low-dose-rate iodine-125 seeds (0.8 mm outer diameter (OD) × 4.5 mm long) were provided by IBt, Inc. (Seneffe, Belgium). One seed was implanted into each tumor. The activity of each seed was 0.5 mCi at the time of implantation (negligible for inactive seeds used for control experiments).

For one group of tumors ($n = 16$), the pO_2 was monitored daily by EPR oximetry using a low-frequency EPR spectrometer (1.2 GHz) (29). The EPR oxygen sensor was a cylindrically shaped 0.9-mm-diameter "plug" of moistened Carlo Erba charcoal. This plug of charcoal was implanted into the center of the tumor, with the trajectory of the implantation running parallel to the mouse leg. The mouse was then allowed to recover for 24 h before further manipulations, to ensure the high stability and reproducibility of the charcoal oxygen sensor (measured previously to be <1 mm Hg variation over 4 months) (30). The iodine-125 seed was subsequently implanted next to and parallel to the plug of charcoal, such that the long axis of the iodine-125 seed was also parallel to the mouse leg. For one subgroup of these tumors ($n = 7$), the iodine-125 seed was implanted within 2 mm of the oxygen sensor (5 active seeds, 2 controls) (Fig. 1a). For another subgroup ($n = 9$), the iodine-125 seed was implanted at a distance of 2 to 4 mm from the oxygen sensor (6 active seeds, 3 controls) (Fig. 1b). Measurements of pO_2 were carried out at 0, 1, 2, 3, and 6 days after implantation of the iodine-125 seed.

For another group of tumors ($n = 17$; 9 radioactive seeds + 8 controls), perfusion was monitored on Days 0, 1, 2, 3, and 6 after iodine-125 seed implantation via single-slice dynamic contrast-enhanced MRI at 4.7 T using the rapid-clearance blood pool agent P792 (Vistarem, Laboratoire Guerbet, Aulnay-sous-Bois, France) (31). For these experiments, the iodine-125 seed was implanted approximately 2 to 3 mm from the tumor center, with the same

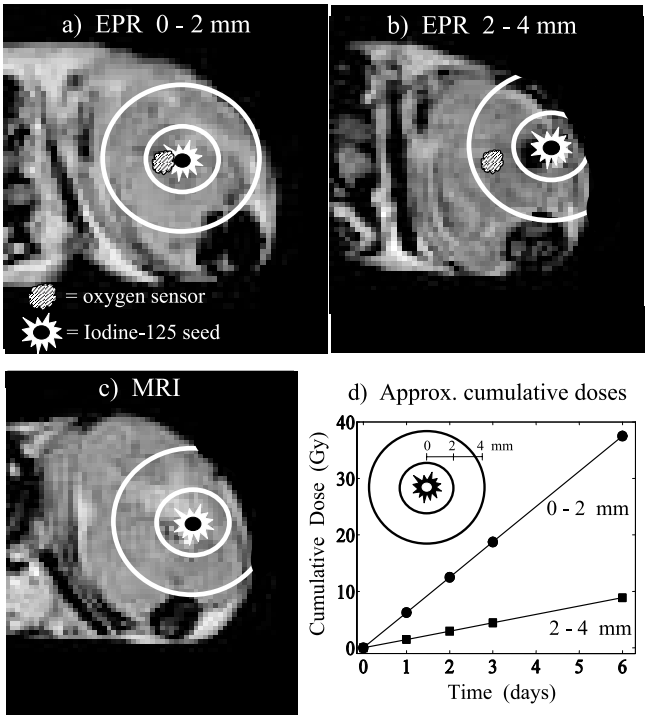

Fig. 1. (a–c) Schematic diagrams showing the relative locations of the tumor, oxygen sensor, and iodine-125 seed for the electron paramagnetic resonance (EPR) and magnetic resonance imaging (MRI) brachytherapy experiments. Each image is a transverse (axial) slice of the tumor. The two white rings surrounding the iodine-125 seed represent distances of 2 and 4 mm from the seed. (d) Approximate cumulative dose as a function of time for the spatial regions of 0–2 mm and 2–4 mm from the iodine-125 seed.

spatial orientation as was employed for the EPR experiments (Fig. 1c). The transverse (axial) slice prescribed in the tumor was chosen to intersect with the center of the iodine-125 seed. (The long axis of the seed was therefore normal to the imaging plane.) High-resolution multislice T_2-weighted spin echo anatomic imaging was performed just before dynamic contrast-enhanced imaging so that the tumor slice could be chosen to co-register as much as possible with the slice used on the previous day. Pixel-by-pixel values for K^{trans} (influx volume transfer constant, from plasma into the interstitial space, units of min^{-1}), v_p (blood plasma volume per unit volume of tissue, unitless), and k_{ep} (fractional rate of efflux from the interstitial space back to blood, units of min^{-1}) in tumor were calculated via tracer kinetic modeling of the dynamic contrast-enhanced data (31). Statistical significance for v_p or K^{trans} identified "perfused" pixels (i.e., pixels to which the contrast agent P792 had access) (31, 32). The resulting parametric maps for K^{trans}, v_p, k_{ep}, and perfused pixels were divided into two regions, or "rings:" One ring contained all the pixels in the tumor located within 2 mm of the iodine-125 seed; the other ring contained all the pixels in the tumor that were located 2 to 4 mm from the iodine-125 seed (Fig. 1c).

The rationale for the two spatial zones—0–2 mm and 2–4 mm from the seeds—was to study how pO_2 and perfusion would react to differing dose rates. This is an important issue in LDR brachytherapy, where the dose rate changes significantly as a function of distance from the seed. In the region <2 mm from the iodine-125 seed, we estimated that the mean dose rate was approximately 6 Gy/day, whereas for 2–4 mm the mean dose rate was estimated to be about 1.5 Gy/day (Fig. 1d). These mean dose rate values were

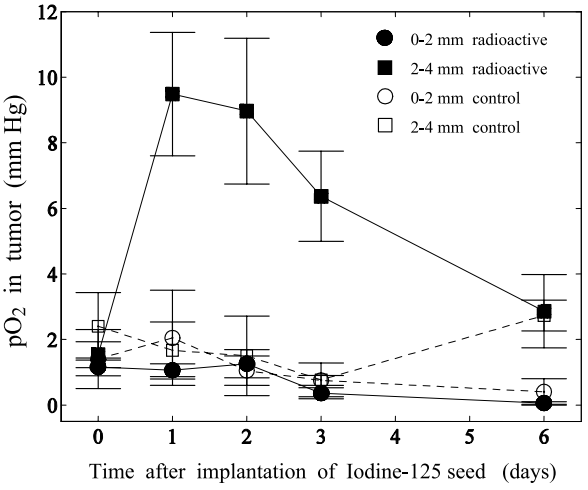

Fig. 2. Electron paramagnetic resonance–derived partial pressure of oxygen in murine transplantable liver tumors, as a function of distance from a 0.5 mCi iodine-125 seed (0–2 or 2–4 mm) and as a function of time (0–6 days after implantation of the seeds). "Control" seeds were not radioactive (0.0 mCi). Results shown are mean ± standard error.

calculated in two steps: First, the dose rate as a function of distance from the seed (up to 10 mm) was calculated by assuming a uniform, cylindrical, source. These dose rates were confirmed at 5 mm and 10 mm with the TG43 recommendations for this seed (33). Second, these dose rates were integrated over spatial elements for <2 mm and 2–4 mm to obtain the mean dose rates for those two regions. The uncertainty in the calculation for the 2–4 mm region was approximately 0.3 Gy/day. For the <2 mm region, the uncertainty was much higher, largely because the exact dose rate depends very strongly on the precise internal structure of each seed. The value of 6 Gy/day is probably an underestimate, with the actual value possibly a factor of 2 or more higher.

Both the EPR pO_2 study and the MRI perfusion study were performed in a longitudinal fashion, i.e., each tumor was followed through the 6 days of brachytherapy treatment.

As mentioned above, the dose rates during delivery of LDR brachytherapy radiation are approximately 3 orders of magnitude smaller than for EBRT. Therefore, the data obtained in this study on the tumor microenvironment during LDR brachytherapy have no true precedent in the literature. To obtain some sort of experimental confirmation of our LDR brachytherapy data, we performed two additional studies with "low dose" EBRT. For the first of these studies, TLT tumors were irradiated with a single dose of only 2 Gy EBRT, followed by pO_2 monitoring via EPR every hour for 6 h, plus one additional EPR measurement at 24 h (n = 6 irradiated tumors + 6 nonirradiated controls) (34). The second additional study (n = 7) was similar to the first one, except that the 2 Gy was divided into 10 separate 0.2 Gy fractions, with approximately 40 min between each fraction (in an effort to "simulate" brachytherapy). The EBRT was performed with 250 keV X-rays (RT 250 irradiator, Philips Medical Systems [Nijmegen, The Netherlands], 1.2 Gy/min). For the irradiations, the tumors were centered in a 3-cm-diameter circular irradiation field.

An additional series of brachytherapy experiments was performed to investigate histologic characteristics of tumor tissue near the iodine-125 seed. For these experiments, radioactive or control seeds were implanted into tumors for varying times (0, 1, 2, 3, or 6 days, n = 5 radioactive experiments per time group, n = 3 controls per time group). At the end of the specified time, the tumor was excised and cut into ~1-mm-thick slices. This cutting was performed such that the plane of each slice was normal to the long axis of the iodine-125 seed (approximately the same orientation as the images in the MRI study). Tumor slices were fixed in formalin, embedded in paraffin, and stained with hematoxylin and eosin. For each tumor, only slides with tumor tissue coinciding with the location of the iodine-125 seed were selected for viewing. These slides were identified as having a single, complete, round, 1–2 mm smooth-edged hole in the tumor tissue (left by the presence of the iodine-125 seed). Each hole was typically larger than the actual iodine-125 seed, as a result of histologic processing and jarring of the tissue during tumor removal and cutting.

RESULTS

Figure 2 shows the results of the EPR pO_2 brachytherapy experiments. For most of the experiments, including all controls, the tumors remained very hypoxic ($pO_2 < 3$ mm Hg) for all time points. The experiments performed with radioactive seeds located at 2–4 mm from the oxygen sensor (configuration shown in Fig. 1b), however, showed an early, significant increase in pO_2 within 24 h ($p < 0.013$, paired Student's t test). The pO_2 for these particular experiments remained significantly higher than the pO_2 for all the other experiments through Day 3 ($p < 0.03$ for each day, Student's t test), then returned to hypoxic levels by Day 6.

Figure 3 shows maps of perfused pixels for four different tumors (two with radioactive seeds, two controls), as a function of time. Qualitatively, it appears that the fraction of perfused pixels in the control tumors gradually decreased with time, whereas that for the tumors with radioactive seeds increased somewhat or remained stable. Figure 4a

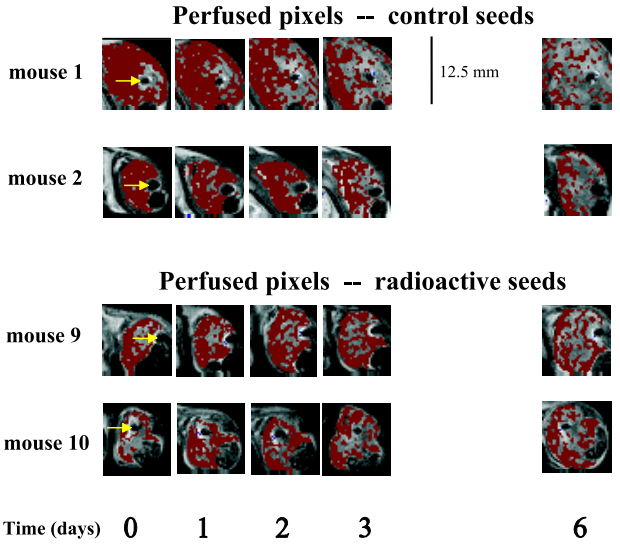

Fig. 3. Example maps of perfused pixels for murine transplantable liver tumors, as a function of time after implantation of an iodine-125 seed (0.0 mCi for control seeds, 0.5 mCi for active seeds). Each map is a T_2-weighted anatomic image overlaid by a binary red map indicating the locations of perfused pixels (for online version only: red = perfused with the contrast agent P792, no red = not perfused). The locations of the seeds on Day 0 are shown by the arrows.

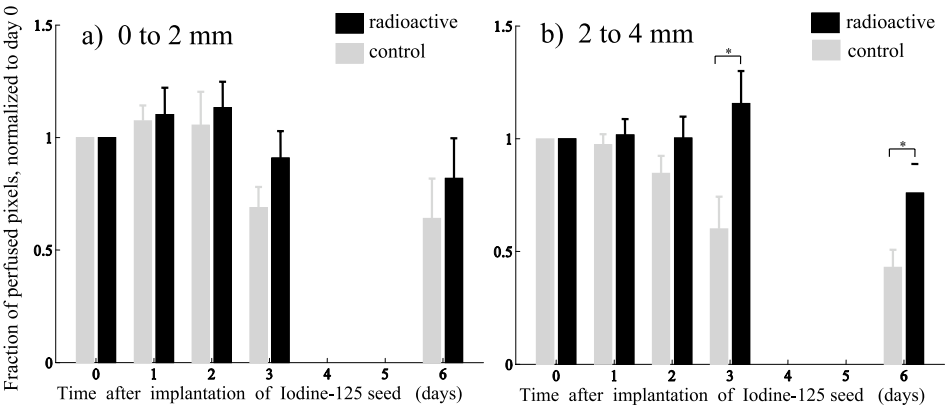

Fig. 4. The fraction of perfused pixels (number of tumor pixels perfused with the contrast agent P792 divided by total number of tumor pixels in the region of investigation) for murine transplantable liver tumors, as a function of distance from an iodine-125 seed (a, 0–2 mm and b, 2–4 mm) and as a function of time (0–6 days after implantation of the seeds), normalized to Day 0. Results shown are the average for all mouse experiments ± standard error. The normalization to Day 0 was performed for each individual mouse before averaging together the data for all mice. *$p < 0.05$, Student's t test

shows the results of quantitative analysis of the fraction of perfused pixels (average of all experiments) for the tumor regions located at 0–2 mm from the iodine-125 seed. Although the fraction of perfused pixels increased more for the tumors with active seeds than for controls, this was not statistically significant at any time point. Figure 4b shows the results for the tumor regions located at 2–4 mm from the iodine-125 seed. Starting on Day 3, the fraction of perfused pixels for the tumors with active seeds was significantly higher than for controls ($p < 0.05$ for each day, Student's t test). No differences in the average values of K^{trans}, v_p, or k_{ep} were observed between tumors with active seeds and tumors with control seeds.

Figures 5 and 6 show the results of the EPR pO_2 EBRT experiments. As shown in Fig. 5, a single dose of 2 Gy EBRT led to a significant increase in pO_2 within 1 h ($p = 0.028$, paired Student's t test). The pO_2 remained significantly elevated for at least 24 h ($p < 0.04$). For the control experiments (data not shown), the pO_2 did not undergo any significant changes with time ($p > 0.1$, paired Student's t test). Figure 6 shows the evolution of the pO_2 during the fractionated EBRT protocol delivering the same total dose of 2 Gy. After 4 fractions of 0.2 Gy (time = 3 h, 0.8 Gy total) the pO_2 began to increase, although not significantly ($p = 0.23$, paired Student's t test). After 7 fractions of 0.2 Gy (time = 5.5 h, 1.4 Gy total), the increase in pO_2 over the baseline value was almost statistically significant ($p = 0.055$). After the completion of the fractionated protocol (time ≥8 h, 2 Gy total), the pO_2 values were significantly elevated relative to the baseline value ($p < 0.002$).

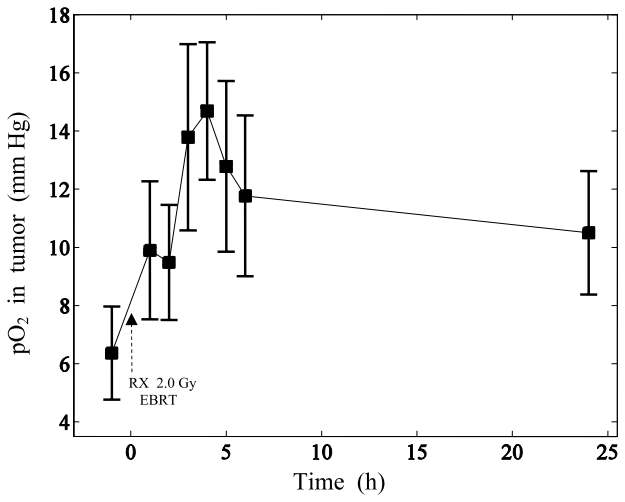

Fig. 5. Electron paramagnetic resonance–derived partial pressure of oxygen in murine transplantable liver tumors, as a function of time after a single dose of 2 Gy external beam radiation therapy. Results shown are mean ± standard error.

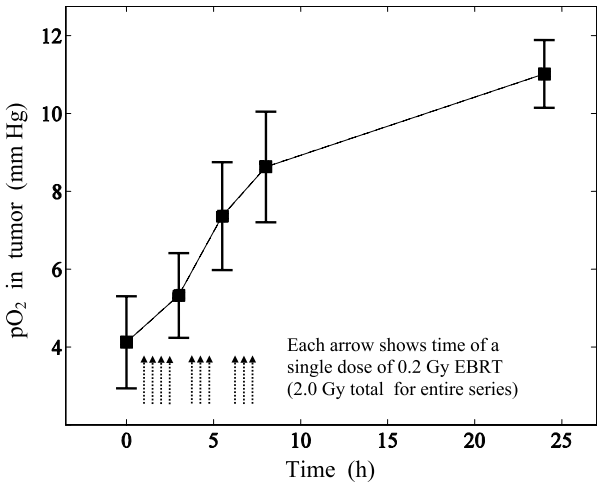

Fig. 6. Electron paramagnetic resonance–derived partial pressure of oxygen in murine transplantable liver tumors, as a function of time during and after a fractionated schedule of external beam radiation therapy (10 fractions of 0.2 Gy for a total of 2.0 Gy). Results shown are mean ± standard error.

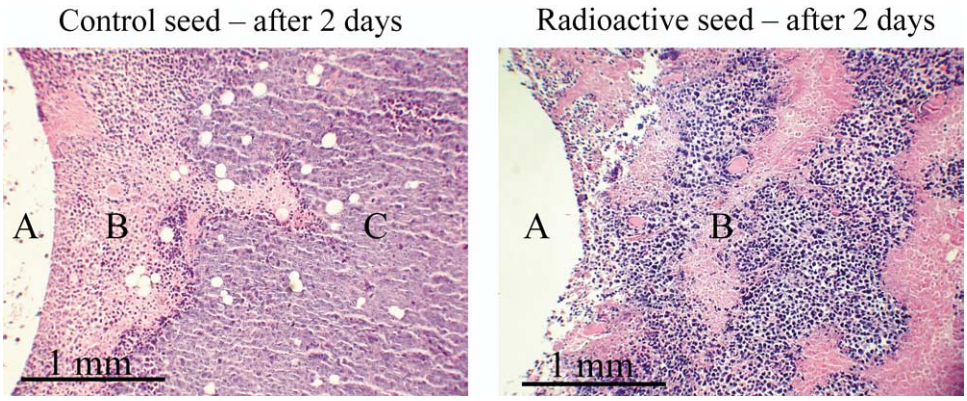

Fig. 7. Images of hematoxylin- and eosin-stained tumor tissue located directly adjacent to iodine-125 seeds (implantation duration = 2 days). (A) Hole left by the iodine-125 seed. (B) Region of mostly dead tumor cells. (C) Region where most tumor cells are intact and alive. Magnification 100×.

Figure 7 shows representative histologic images of tumor tissue which was adjacent to the iodine-125 seeds (implantation duration = 2 days). For the image on the left (a control), the hole left by the iodine-125 seed (A) is rimmed by a 1–2 mm-thick zone of dead tumor cells characterized by hyperchromatic nuclei and intensely eosin-staining cytoplasm (B). Farther out, most tumor cells are intact and alive (C). For the image on the right (radioactive seed), the hole left by the iodine-125 seed (A) is surrounded by a large region of cellular necrosis (B) characterized by isolated pycnotic nuclei, cellular debris, and intensely eosin-staining fibrous tissue. Far beyond the hole (>4 mm, not shown), the tumor cells are once again mostly intact and alive. We did not observe any evidence of inflammation on any of the slides studied.

DISCUSSION

In this work we report, for the first time, measurements of tumor pO_2 and blood perfusion as a function of time after implantation of radioactive iodine-125 seeds used in LDR brachytherapy. At distances of 2–4 mm from the radioactive iodine-125 seeds, both pO_2 and blood perfusion were observed to increase relatively shortly after implantation of the seed (within ~24 and 72 h, respectively). The pO_2 remained elevated (>6–9 mm Hg) through Day 3.

These results are not totally surprising. Increases in tumor oxygenation and perfusion shortly after a single, large (> ~10 Gy) dose of EBRT have been observed by other investigators (15–24). However, some caution should be observed when comparing such EBRT data with these new LDR brachytherapy data. LDR brachytherapy and EBRT differ considerably in terms of dose rate and homogeneity of the radiation field within the tumor. It is possible, therefore, that these two radiation treatments may affect the tumor microenvironment in different ways.

In the region of 2–4 mm from the radioactive iodine-125 seed, a small dose (~1.5 Gy total) was delivered continuously to the tumor over 24 h, resulting in a significant increase in pO_2. Strictly in terms of total dose delivered over 24 h, these data are consistent with the two supplemental EBRT experiments which we performed (Figs. 5 and 6). What is interesting is that the pO_2 increased regardless of how this small dose was delivered: as a single dose (Fig. 5), in a fractionated schedule (Fig. 6), or continuously (Fig. 2). It may be noted that the basal (preirradiation) tumor pO_2 differed somewhat for these three experiments: ~2 mm Hg for the brachytherapy experiments, ~6 mm Hg for the single-dose EBRT experiments, and ~4 mm Hg for the fractionated EBRT experiments. These three experiments were performed on three different groups of tumors, however, with several months of separation. Moreover, such differing values are not contrary to our experience with TLT mouse tumors (dozens of groups spanning several years): the average basal pO_2 has indeed been observed to vary somewhat from group to group (range 2 to 10 mm Hg), probably because of subtle differences in tumor architecture resulting from minor variations in the inoculation procedure (exact location of tumor implantation, number of cells, etc.).

In the region of 2–4 mm from the radioactive iodine-125 seed, there was a delay between the increase in pO_2 and the increase in perfusion. Therefore, the early increase in pO_2 (at 24 h) is probably due primarily to a decrease in oxygen consumption rather than to an increase in perfusion. This is in contrast to previous EBRT work performed by our group, where it was found that the early increase in pO_2 after a single dose of 2 Gy EBRT (as in Fig. 5) was in all likelihood partly caused by an increase in perfusion resulting from inflammation (34). The lack of an early increase in perfusion in the current study therefore suggests that the extremely low dose rates delivered by LDR brachytherapy are less able to cause inflammation. This hypothesis is supported by our histologic data, which showed no evidence of inflammation.

Assuming that oxygen consumption decreases for the region of 2–4 mm from the radioactive iodine-125 seed, this decrease could simply be the result of there being fewer viable cells, many of the cells having been killed by the

radiation. This cell killing can be seen in Fig. 7 by comparing the image from the control experiment (left image, intact alive tumor cells in region C) with the image from the radioactive experiment (right image, most cells dead). The reduction in the number of viable cells could eventually reduce pressure on the capillaries, which would allow perfusion to increase (34, 35). This would explain the observed delay between the pO_2 increase and the perfusion increase. Unfortunately, validating these hypotheses could be difficult. Current methods for measuring oxygen consumption and interstitial fluid pressure are whole-tumor techniques and may not be easily adapted for making measurements in small, precisely localized regions of the tumor.

For untreated tumors, a general decline in perfusion as a function of time (e.g., Figure 4 controls) is a phenomenon which has been observed by many groups in a variety of tumor models (36–45). The generally accepted explanation is that as a tumor grows and angiogenesis continues, the capillaries that transport blood from major vessels to the main tumor mass become longer and longer, resulting in higher blood flow resistance and greater diffusion distances for nutrients (36–38). In addition, proliferating cancer cells may compress capillaries, further reducing perfusion (35). Eventually, most of the tumor will become less and less perfused, with the exception of the exterior (rim) which has short, easy access to normal tissue capillaries (36). The end result is that the fraction of total tumor mass which is well-perfused decreases with time (36, 39).

No significant changes in pO_2 were observed in the region of 0–2 mm from the iodine-125 seed (~6 Gy/day). This lack of response is probably related to mechanical damage of the tumor tissue in and around the oxygen sensor caused by implantation of the iodine-125 seed. Indeed, the histologic data showed a rim of cell death (thickness 1–2 mm) around all iodine-125 seeds, radioactive or control. Fortunately, this issue is not likely to have important clinical consequences, because the tumor tissue in this region receives extremely high cumulative doses (~250 to 500 Gy total over the entire course of treatment).

There may be clinical consequences, however, for the observations we made in the region of 2–4 mm from the iodine-125 seed, where the doses delivered are much lower than for the 0–2 mm region. The 2–4 mm region corresponds approximately to the spatial zone between seeds implanted in tumors clinically (~5 to 10 mm spacing between seeds). Assuming that human tumors react to LDR brachytherapy radiation in the same way that TLT murine tumors do, our data indicate that it may be advantageous to give adjuvant EBRT shortly (e.g., 1 or 2 days) after commencement of LDR brachytherapy. At that time, the pO_2 in the spatial regions between seeds should be elevated, which will radiosensitize the tumor cells in those regions. If chemotherapy is given adjuvantly, it may best be administered just a little later (e.g., 3 or 4 days) after the start of LDR brachytherapy. At that time, perfusion should be elevated, permitting better penetration of the drug into the tumor.

CONCLUSIONS

In this article we report, for the first time, measurements of tumor pO_2 and blood perfusion as a function of time after implantation of 0.5 mCi iodine-125 seeds used in LDR brachytherapy. At distances of 2–4 mm from the seeds (dose rate = ~1.5 Gy per day), both pO_2 and blood perfusion were observed to increase relatively shortly after implantation of the seed (within ~24 and 72 h, respectively).

These data may have ramifications for the clinical use of LDR brachytherapy, where external radiation or chemotherapy may be used adjuvantly. The data suggest that it could be advantageous to give adjuvant external radiation shortly (e.g., 1 or 2 days) after commencement of LDR brachytherapy. At that time, the pO_2 in the spatial regions between seeds could be elevated, which would radiosensitize the tumor cells in those regions. If chemotherapy is given adjuvantly, it may best be administered just a little later (e.g., 3 or 4 days) after the start of LDR brachytherapy. At that time, perfusion could be elevated, permitting better penetration of the drug into the tumor.

REFERENCES

1. Vicini FA, Kini VR, Edmundson G, *et al.* A comprehensive review of prostate cancer brachytherapy: Defining an optimal technique. *Int J Radiat Oncol Biol Phys* 1999;44:483–491.
2. Langley SEM, Laing R. Prostate brachytherapy has come of age: A review of the technique and results. *BJU International* 2002;89:241–249.
3. Bladou F, Salem N, Simonian-Sauve M, *et al.* Permanent iodine 125 implant brachytherapy in localized prostate cancer: Results of the first 4 years of experience. *Prog Urol* 2004;14: 345–352.
4. DiBiase SJ, Hosseinzadeh K, Gullapalli RP, *et al.* Magnetic resonance spectroscopic imaging-guided brachytherapy for localized prostate cancer. *Int J Radiat Oncol Biol Phys* 2002; 52:429–438.
5. Ghaly M, Wallner K, Merrick G, *et al.* The effect of supplemental beam radiation on prostate brachytherapy-related morbidity: Morbidity outcomes from two prospective randomized multicenter trials. *Int J Radiat Oncol Biol Phys* 2003;55: 1288–1293.
6. Roach M. "Supplemental beam" and prostate brachytherapy: A simple answer to a complicated question? *Int J Radiat Oncol Biol Phys* 2003;55:1162–1163.
7. Lee WR. In regard to Ghaly *et al.*, IJROBP 2003;55:1288–1293 [Letter]. *Int J Radiat Oncol Biol Phys* 2003;57:1198.
8. Wallner K, Merrick G, Ghaly M. In response to Dr. Lee [Letter]. *Int J Radiat Oncol Biol Phys* 2003;57:1198–1199.
9. Brown JM, Giaccia AJ. The unique physiology of solid tumors: Opportunities (and problems) for cancer therapy. *Cancer Res* 1998;58:1408–1416.
10. van den Berg AP, van Geel CA, van Hooije CM, *et al.* Tumor hypoxia—a confounding or exploitable factor in interstitial brachytherapy? Effects of tissue trauma in an experimental rat tumor model. *Int J Radiat Oncol Biol Phys* 2000;48:233–240.

11. Mayr NA, Yuh WT, Arnholt JC, *et al.* Pixel analysis of MR perfusion imaging in predicting radiation therapy outcome in cervical cancer. *J Magn Reson Imaging* 2000;12:1027–1033.
12. Hill RP, Fyles W, Milosevic M, *et al.* Is there a relationship between repopulation and hypoxia/reoxygenation? Results from human carcinoma of the cervix. *Int J Radiat Biol* 2003; 79:487–494.
13. Movsas B, Chapman JD, Hanlon AL, *et al.* Hypoxic prostate/muscle pO_2 ratio predicts for biochemical failure in patients with prostate cancer: Preliminary findings. *Urology* 2002;60: 634–639.
14. Knocke TH, Weitmann HD, Feldmann HJ, *et al.* Intratumoral pO_2-measurements as predictive assay in the treatment of carcinoma of the uterine cervix. *Radiother Oncol* 1999;53:99–104.
15. O'Hara JA, Goda F, Liu KJ, *et al.* The pO_2 in a murine tumor after irradiation: An in vivo electron paramagnetic resonance oximetry study. *Radiat Res* 1995;144:222–229.
16. O'Hara J, Goda F, Demindenko E, *et al.* Effect on regrowth delay in a murine tumor scheduling split dose irradiation based on direct pO_2 measurements by electron paramagnetic resonance oximetry. *Radiat Res* 1998;150:549–556.
17. Goda F, O'Hara JA, Rhodes ES, *et al.* Changes of oxygen tension in experimental tumors after a single dose of X-ray irradiation. *Cancer Res* 1995;55:2249–2252.
18. Goda F, Bacic G, O'Hara JA, *et al.* The relationship between pO_2 and perfusion in two murine tumors after X-ray irradiation: A combined Gd-DTPA dynamic MRI and EPR oximetry study. *Cancer Res* 1996;56:3344–3349.
19. Vaupel P, Frinak S, O'Hara M. Direct measurement of reoxygenation in malignant mammary tumors after a single large dose of irradiation. *Adv Exp Med Biol* 1984;180:773–782.
20. Koutcher JA, Alfieri AA, Devitt ML, *et al.* Quantitative changes in tumor metabolism, partial pressure of oxygen, and radiobiological oxygenation status postradiation. *Cancer Res* 1992;52:4620–4627.
21. Fenton B, Lord E, Paoni S. Effect of radiation on tumor intravascular oxygenation, vascular configuration, development of hypoxia, and clonogenic survival. *Radiat Res* 2001; 155:360–368.
22. Mason RP, Hunjan S, Le D, *et al.* Regional tumor oxygen tension: Fluorine echo planar imaging of hexafluorobenzene reveals heterogeneity of dynamics. *Int J Radiat Oncol Biol Phys* 1998;42:747–750.
23. Olive PL. Radiation-induced reoxygenation in the SCCVII murine tumour: Evidence for a decrease in oxygen consumption and an increase in tumour perfusion. *Radiother Oncol* 1994;32:37–46.
24. Sonveaux P, Dessy C, Brouet A, *et al.* Modulation of the tumor vasculature functionality by ionizing radiation accounts for tumor radiosensitization and promotes gene delivery. *FASEB J* 2002;16:1979–1981.
25. Fan X, Medved M, River JN, *et al.* New model for analysis of dynamic contrast-enhanced MRI data distinguishes metastatic from nonmetastatic transplanted rodent prostate tumors. *Magn Reson Med* 2004;51:487–494.
26. Tofts PS. Modeling tracer kinetics in dynamic Gd-DTPA MR imaging. *J Magn Reson Imaging* 1997;7:91–101.
27. Gallez B, Baudelet C, Jordan BF. Assessment of tumor oxygenation by electron paramagnetic resonance: Principles and applications. *NMR Biomed* 2004;17:240–262.
28. Taper HS, Woolley GW, Teller MN, *et al.* A new transplantable mouse liver tumor of spontaneous origin. *Cancer Res* 1966;26:143–148.
29. Gallez B, Jordan BF, Baudelet C, *et al.* Pharmacological modifications of the partial pressure of oxygen in murine tumors: Evaluation using in vivo EPR oximetry. *Magn Reson Med* 1999;42:627–630.
30. Jordan BF, Baudelet C, Gallez B. Carbon-centered radicals as oxygen sensors for in vivo electron paramagnetic resonance: Screening for an optimal probe among commercially available charcoals. *MAGMA* 1998;7:121–129.
31. Baudelet C, Ansiaux R, Jordan BF, *et al.* Physiological noise in murine solid tumours using T2*-weighted gradient-echo imaging: A marker of tumour acute hypoxia? *Phys Med Biol* 2004;49:3389–3411.
32. Galbraith SM, Maxwell RJ, Lodge MA, *et al.* Combretastatin A4 phosphate has tumor antivascular activity in rat and man as demonstrated by dynamic magnetic resonance imaging. *J Clin Oncol* 2003;21:2831–2842.
33. Reniers B, Vynckier S, Scalliet P. Dosimetric study of the new InterSource^{125} iodine seed. *Med Phys* 2001;28:2285–2288.
34. Crokart N, Jordan BF, Baudelet C, *et al.* Early reoxygenation in tumors after irradiation: Determining factors and consequences for radiotherapy regimens using multiple fractions per day. *Int J Radiat Oncol Biol Phys*. 2005;63:901–910.
35. Padera TP, Stoll BR, Tooredman JB, *et al.* Pathology: Cancer cells compress intratumour vessels. *Nature* 2004;427:695.
36. Baker GM, Goddard HL, Clarke MB, *et al.* Proportion of necrosis in transplanted murine adenocarcinomas and its relationship to tumor growth. *Growth Dev Aging* 1990;54:85–93.
37. Sevick EM, Jain RK. Geometric resistance to blood flow in solid tumors perfused ex vivo: Effects of tumor size and perfusion pressure. *Cancer Res* 1989;49:3506–3512.
38. Lyng H, Skretting A, Rofstad EK. Blood flow in six human melanoma xenograft lines with different growth characteristics. *Cancer Res* 1992;52:584–592.
39. Khalil AA, Horsman MR, Overgaard J. The importance of determining necrotic fraction when studying the effect of tumour volume on tissue oxygenation. *Acta Oncol* 1995;34: 297–300.
40. Sundqvist K, Hafstrom L, Persson B. Measurements of total and regional tumor blood flow and organ blood flow using 99Tcm labelled microspheres: An experimental study in rats. *Eur Surg Res* 1978;10:433–443.
41. Siracka E, Pappova N, Pipa V, *et al.* Changes in blood flow of growing experimental tumor determined by the clearance of 133Xe. *Neoplasma* 1979;26:173–177.
42. Baredes S, Kim S. Distribution of blood flow in an experimental palatal carcinoma. *Am J Otolaryngol* 1988;9:155–160.
43. Tozer GM, Lewis S, Michalowski A, *et al.* The relationship between regional variations in blood flow and histology in a transplanted rat fibrosarcoma. *Br J Cancer* 1990;61:250–257.
44. Su MY, Wang Z, Nalcioglu O. Investigation of longitudinal vascular changes in control and chemotherapy-treated tumors to serve as therapeutic efficacy predictors. *J Magn Reson Imaging* 1999;9:128–137.
45. Kiessling F, Heilmann M, Vosseler S, *et al.* Dynamic T1-weighted monitoring of vascularization in human carcinoma heterotransplants by magnetic resonance imaging. *Int J Cancer* 2003;104:113–120.